System-size dependence of γ-jet modifications in heavy-ion collisions*

Yu-Xin Xiao (肖宇昕)[1] Qing-Fei Han (韩庆飞)[1] He-Xia Zhang (张贺霞)[2†] Han-zhong Zhang (张汉中)[1‡]

[1]Key Laboratory of Quark & Lepton Physics (MOE) and Institute of Particle Physics, Central China Normal University, Wuhan 430079, China
[2]Key Laboratory of Information Functional Material for Fujian Higher Education, College of Physics and Information Engineering, Quanzhou Normal University, Quanzhou 362000, China

Abstract: Medium modifications of γ-triggered jets are investigated with the linear Boltzmann transport model in heavy-ion collisions with varying system sizes, focusing on centrality dependence in Pb+Pb and Xe+Xe collisions at the LHC. Our numerical results reveal that jets produced in central collisions exhibit a wider transverse asymmetry (A_N^y) distribution, broader jet shape, and more pronounced γ-jet transverse momentum imbalance ($X_{J\gamma} = p_T^{\rm jet}/p_T^{\gamma}$) compared with peripheral collisions. These effects arise from the longer path length and stronger jet-medium interactions in central collisions, leading to enhanced jet quenching and medium response. Our findings demonstrate that the magnitude of γ-jet modifications is sensitive to the size and centrality of the collision system, with larger systems inducing more significant alterations owing to increased energy loss and medium feedback.

Keywords: jet quenching, medium modification, LBT model, jet shape

DOI: 10.1088/1674-1137/adef24 **CSTR:** 32044.14.ChinesePhysicsC.49124101

I. INTRODUCTION

Over the past 20 years, the Relativistic Heavy Ion Collider (RHIC) at Brookhaven National Laboratory and the Large Hadron Collider (LHC) at CERN have executed a series of experiments on relativistic heavy-ion collisions. These experiments provide an unparalleled experimental environment to explore the properties of matter under strong interactions. One of the most notable discoveries is the formation of a new state of matter, termed the quark gluon plasma (QGP). It is a deconfined phase of quarks and gluons, hypothesized to have existed within the neutron star and in the primordial universe microseconds after the Big Bang.

Jets, which are showers of energetic particles produced by the fragmentation of large transverse partons, serve as a critical tool for examining the characteristics of the QGP medium. In relativistic heavy-ion collisions, jets or high transverse momentum (p_T) partons, generated in the early stage of collisions, propagate through the QGP, undergo multiple scattering interactions with the QGP medium, and experience energy loss. This phenomenon is known as jet quenching [1−3]. This effect has been detected in experiments conducted at both the RHIC [4, 5] and LHC [6−9]. Furthermore, large p_T dihadrons, gamma-hadrons, and dijets show suppression, transverse momentum balance [10], and azimuthal decorrelation [11−15], and the structure of the full jet is significantly altered by the QGP medium [16-19], as evidenced at both the RHIC and LHC [20−24].

Theoretical studies have indicated that the intensity of jet quenching is directly proportional to the jet transport coefficient $\hat{q}$, defined as the averaged transverse momentum broadening squared per unit length along the trajectory of a parton [25−31]. In recent years, studies concerning $\hat{q}$ have gained significant attention [32−38]. The variable $\hat{q}$ has the ability to reflect numerous properties of the QGP medium. It is associated with the energy loss of the jet and is directly linked to the temperature and density of the medium. In the context of heavy-ion collisions, the distribution of $\hat{q}$ and its spatial gradient within an expanding QGP fireball is non-uniform. The temperature and density reach their peak at the center of the fireball, where the value of $\hat{q}$ also attains its maximum. The initial spatial distributions are determined by the nuclear geometry of two colliding nuclei. The subsequent time evolution can be ascertained through a hydrodynamic model, utilizing an initial condition model commonly referenced in previous studies [39−47]. As partons traverse the non-uniform QGP medium, insights into the evolution can be gleaned by examining the final jets. Notably, the two-dimensional (2D) jet tomography technique,

Received 1 May 2025; Accepted 14 July 2025; Published online 15 July 2025

* Supported by National Natural Science Foundation of China (11935007), Guangdong Basic and Applied Basic Research Foundation (2021A1515110817), Guangdong Major Project of Basic and Applied Basic Research (2020B0301030008), and Science and Technology Program of Guangzhou (2019050001)

† E-mail: hxzhang@qztc.edu.cn

‡ E-mail: zhanghz@mail.ccnu.edu.cn

which integrates both transverse [48] and longitudinal [13, 14] tomography methods introduced in our prior study, facilitates the identification of the initial production position of the γ-jets [49].

Jets triggered by gauge bosons, such as photons, are regarded as a "golden channel" among jet quenching observables owing to their distinctive properties. As these bosons are produced in the initial hard scattering process and do not undergo strong interactions with the QGP medium, they serve as an effective probe for studying jet energy loss. By analyzing boson-triggered jets, we can more reliably access the initial transverse momentum of the associated-jet information that would otherwise be obscured by medium interactions. Among the various studies on boson-triggered jets, γ-tagged jets constitute one of the most prominent and well-investigated categories [50−54].

In our previous study [49], we employed 2D jet tomography to select jet events with varying initial production positions on the transverse plane. This approach amplifies the medium modification signatures of γ-jets — including both jet quenching and jet-induced medium response—by concentrating on jets produced at the central region of the QGP medium in 0%−10% Pb+Pb collisions at $\sqrt{s_{NN}} = 5.02$ TeV. Our findings reveal that jet modifications in the QGP medium are governed by two key factors: First, they depend on the spatial distribution of the jet transport coefficient $\hat{q}$ within the medium, which determines the jet quenching magnitude and energy loss. The energy dissipated by hard partons is redistributed from the jet core to large-angle regions relative to the jet axis, thereby enhancing the medium response. Second, these modifications correlate with the spatial gradient of the medium density. Given the inhomogeneous distribution of the medium, individual jet partons within the jet cone undergo distinct evolution processes, ultimately generating an asymmetric jet shape.

This framework offers an alternative approach to probe jet modifications by leveraging QGP fireballs of different sizes produced in collisions with varying centralities. In heavy-ion collisions, central collisions create larger, hotter QGP systems, whereas peripheral collisions yield smaller, cooler systems [23, 55−57]. Consequently, jets traversing central collisions exhibit more pronounced quenching and medium-induced modifications compared with peripheral cases. Moreover, system sizes differ across collision species. For example, at fixed centrality, Xe+Xe collisions generate smaller systems than Pb+Pb collisions [58−60]. In this study, we systematically analyze γ-jet modifications across different system scales by comparing centrality-dependent jet observables in Pb+Pb and Xe+Xe collisions. We anticipate that future experimental studies on jet modification and asymmetry will advance our understanding of jet transport properties and medium response dynamics.

The remainder of this paper is organized as follows. Sec. II introduces our framework, specifically the linear Boltzmann transport (LBT) model. Sec. III discusses the medium modification of γ-jets with various centrality intervals in Pb+Pb collisions and Xe+Xe collisions. A summary is provided in Sec. IV.

II. FRAMEWORK

The LBT model [61−66] was developed to investigate the jet propagation within the QGP medium in heavy-ion collisions, which not only describes parton energy loss but also accounts for jet-induced medium excitation. It has been used to describe experimental data on the suppression of single hadrons [63], single jets [67], γ-hadron [68], and γ-jet correlations [69] in heavy-ion collisions at both the RHIC and LHC energies.

In this study, jet propagation (including shower and recoil partons), parton energy loss, and the medium response in the QGP medium due to the interactions between the jet and medium are simulated within the LBT model, which is described by the linear Boltzmann equations,

$$p_a \cdot \partial f_a = \int \prod_{i=b,c,d} \frac{\mathrm{d}^3 p_i}{2E_i(2\pi)^3} \frac{\gamma_b}{2} (f_c f_d - f_a f_b) |\mathcal{M}_{\dashv\lfloor\to\rfloor\Gamma}|^{\in} \times S_2(\hat{s},\hat{t},\hat{u}) 2\pi^4 \delta^4(p_a + p_b - p_c - p_d) + \text{inelastic}, \tag{1}$$

where $|\mathcal{M}_{ab\to cd}|$ is the leading-order elastic scattering amplitude defined by the Mandelstam variables $\hat{s}, \hat{t}$, and $\hat{u}$. $f_i = (2\pi)^3 \delta^3(\boldsymbol{p} - \boldsymbol{p}_i)\delta^3(\boldsymbol{x} - \boldsymbol{x}_i - \boldsymbol{v}_i t)$ is the phase space density for jet partons before $(i = a)$ and after $(i = c)$ scattering. $f_i = 1/(\mathrm{e}^{p_i \cdot u/T} \pm 1)$ is the phase space distribution of thermal partons before $(i = b)$ and after $(i = d)$ scattering in the QGP medium with local temperature T and fluid 4-velocity u. The regularization factor,

$$S_2(\hat{s},\hat{t},\hat{u}) = \theta(\hat{s} \geq 2\mu_D^2)\theta(-\hat{s} + \mu_D^2 \leq \hat{t} \leq -\mu_D^2), \tag{2}$$

is used to avoid the collinear divergence in $|\mathcal{M}_{ab\to cd}|$, and the Debye screening mass is defined as $\mu_D^2 = 3g^2T^2/2$.

In the LBT model, the description of the inelastic processes of medium-induced gluon radiation is based on the high-twist approach [28, 70] with the radiative gluon spectrum,

$$\frac{\mathrm{d}N_g^a}{\mathrm{d}z\mathrm{d}k_\perp^2 d\tau} = \frac{6\alpha_s P_a(z) k_\perp^4}{\pi(k_\perp^2 + z^2 m^2)^4} \frac{p \cdot u}{p_0} \hat{q}_a(x) \sin^2 \frac{\tau - \tau_i}{2\tau_f}, \tag{3}$$

where m is the mass of the propagating parton a, and z and $k_\perp$ are the energy fraction and transverse momentum of the radiated gluon, respectively. The strong coupling

constant is denoted as α_s, and $\hat{q}_a$ represents the jet transport coefficient, which is defined as the squared transverse momentum transfer per unit path length for the parton a traversing through the medium. $P_a(z)$ is the splitting function for $a \to a+g$, and $\tau_f = \frac{2Ez(1-z)}{k_\perp^2+z^2M^2}$ represents the formation time of the radiated gluon [69]. In the LBT model, both the jet shower partons and the recoiled medium partons follow the Boltzmann equation for their transport. After being produced, they undergo further elastic and inelastic scattering processes. The depletion of the medium owing to back-reaction is also considered through "negative" partons whose energy and momentum must be subtracted from the final observables. The recoiled partons and "negative" partons are referred to as the medium-response in our description.

As a fundamental component of our jet propagation framework, the LBT model describes jet evolution within the QGP medium. Our comprehensive simulation integrates multiple theoretical components: the TRENTo initial condition model, (3+1)-dimensional viscous hydrodynamics (CLVisc), PYTHIA8 event generator, and FastJet package. The initial parton shower for γ-jet events is generated using PYTHIA 8 [71, 72]. The TRENTo model [46, 47] provides both the initial energy density distribution and collision geometry, including binary collision counts ($N_{\rm coll}$) that determine γ-jet production positions. These energy density distributions serve as initial conditions for the CLVisc (3+1)-D viscous hydrodynamic evolution [40, 41] of the QGP medium. The LBT model simulates jet parton propagation through the evolving QGP medium, with scattering rates calculated using local temperature and fluid four-velocity from CLVisc at each timestep. The hydrodynamic simulation uses initial time $\tau_0 = 0.6$ fm/c and freeze-out temperature $T_f = 137$ MeV, defining the duration of parton-medium interactions. Final jet reconstruction employs the anti-k_t algorithm implemented in FastJet [73, 74].

In the following calculations, we select the trigger photon with $p_T^\gamma > 60$ GeV/c of γ-jet events in Pb+Pb collisions at $\sqrt{s_{NN}} = 5.02$ TeV and Xe+Xe collisions at $\sqrt{s_{NN}} = 5.44$ TeV. The cone size of the γ-triggered jets is set as $R = 0.3$, and the lower threshold of transverse momentum for the jets is set at $p_T^{\rm jet} > 30$ GeV/c, with associated partons selected with $p_T^{\rm assoc} > 1$ GeV/c. The pseudorapidities for the γ-jets are constrained within $|\eta_\gamma| < 1.44$ and $|\eta_{\rm jet}| < 1.6$, and their azimuthal angle differences $|\Delta\phi_{j\gamma}|$ are restricted to be larger than $(7/8)\pi$. Fig. 1 shows the illustration of the γ-jet configuration relative to the event plane. In all our calculations for Pb+Pb and Xe+Xe collisions, we assume that the event plane is oriented along the x-axis. The wavy arrow pointing toward the negative x-direction denotes the selected trigger photon direction, which lies parallel to the event plane. Correspondingly, the associated jet is approximately

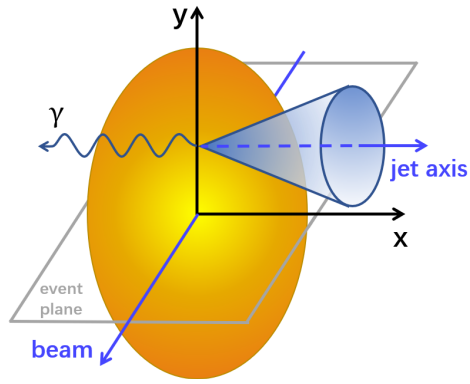

Fig. 1. (color online) Illustration of the γ-jet configuration relative to the event plane

aligned along the positive x-axis, as illustrated by the cone in Fig. 1. On the one hand, unifying the initial directions of the jets can prevent the values of A_N^n from being averaged out statistically, which is crucial for the calculation of A_N^n. On the other hand, constraining the initial directions of the jets helps us better regulate the paths of jet propagation through the QGP. This enables us to study the jet quenching effect relying on the propagation path more directly.

III. JET TOMOGRAPHY WITHIN DIFFERENT SYSTEM SIZES VIA PB+PB AND XE+XE COLLISIONS

A. Jet modification of γ-jet in Pb+Pb collisions

Owing to the non-uniform QGP medium, an asymmetry of the jet denoted as A_N^n caused by the gradient of the medium density (or the $\hat{q}$ gradient) can be introduced to localize the initial position of jet production perpendicular to the propagation direction, when it propagates through the QGP medium [48]. The asymmetry A_N^n used for transverse jet tomography is defined as,

$$A_N^n = \frac{\sum_a \int {\rm d}^3r{\rm d}^3k f_a(\boldsymbol{k},\boldsymbol{r}) {\rm Sign}(\boldsymbol{k}\cdot\boldsymbol{n})}{\sum_a \int {\rm d}^3r{\rm d}^3k f_a(\boldsymbol{k},\boldsymbol{r})}, \tag{4}$$

where f_a is the phase-space distribution of partons, and $\boldsymbol{n}$ denotes the normal direction of the plane, which is defined by the beam direction and the direction of the trigger particle as the positive y-axis in our set-up shown in Fig. 1. We sum up all the partons inside a jet.

We first examined the transverse asymmetry (A_N^y) distribution in Pb+Pb collisions across different centrality intervals. As shown in Fig. 2, our numerical results demonstrate the γ-jet production rates as functions of A_N^y

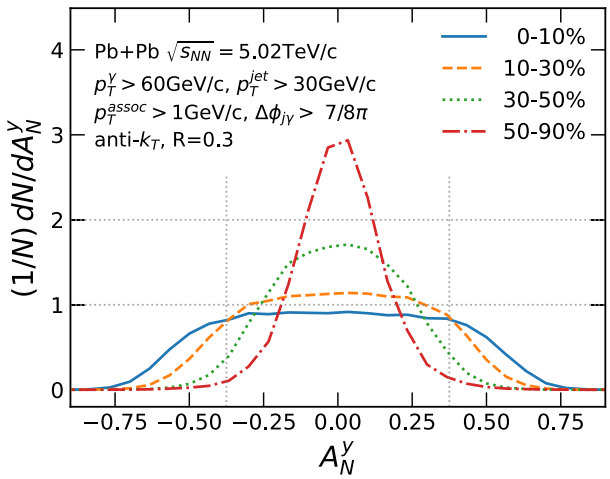

Fig. 2. (color online) γ-jet production rates $(1/N)\mathrm{d}N/\mathrm{d}A_N^y$ as functions of A_N^y, with four centrality intervals, specifically 0%−10%, 10%−30%, 30%−50%, and 50%−90%, in Pb+Pb collisions at $\sqrt{s_{NN}}$ = 5.02 TeV

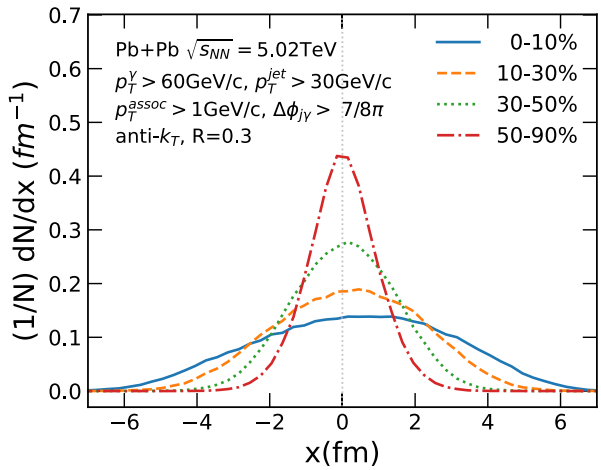

Fig. 3. (color online) γ-jet production rates $(1/N)\mathrm{d}N/\mathrm{d}x$ as functions of the initial jet production position x, with four centrality intervals, specifically 0%−10%, 10%−30%, 30%−50%, and 50%−90%, in Pb+Pb collisions at $\sqrt{s_{NN}}$ = 5.02 TeV

for four centrality classes (0%−10%, 10%−30%, 30%−50%, and 50%−90%) in Pb+Pb collisions at $\sqrt{s_{NN}}$ = 5.02 TeV. The A_N^y distribution exhibits greater broadening in central collisions compared with that in peripheral collisions. As the collision system transitions from central to peripheral configurations, the A_N^y distribution progressively narrows. This observation suggests that jets propagating parallel to the event plane show higher transverse asymmetry in central collisions than in peripheral collisions. In central collisions, jets traversing the QGP experience longer propagation paths, which lead to more pronounced jet quenching effects. These mechanisms lead to substantial medium-induced jet modifications, consequently producing more significant jet asymmetry.

Fig. 3 shows the γ-jet production rates as functions of the initial jet production position x with different centrality intervals, specifically 0%−10%, 10%−30%, 30%−50%, and 50%−90%, in Pb+Pb collisions at $\sqrt{s_{NN}}$ = 5.02 TeV. The results demonstrate the variation in system size along the x-axis between central and peripheral collisions. Central collisions exhibit a broader initial jet production position distribution, corresponding to a larger collision system size, whereas peripheral collisions show a narrower distribution, indicating a smaller system size. Furthermore, the enhanced jet quenching effect in central collisions leads to more pronounced surface emission of jets, resulting in an asymmetric initial jet production position distribution with a distinct shift toward the positive x-axis direction (Fig. 3). As the collision centrality decreases (from central to peripheral), the jet quenching strength weakens, causing the x-position distributions to gradually regain symmetry and become narrower. This observation is consistent with the conclusions from our previous study on longitudinal jet tomography [13, 14, 49].

The jet shape, which characterizes the transverse momentum distribution of particles within the jet cone relative to the jet axis, serves as a crucial observable for investigating jet transport properties and medium response. It is defined as the probability density function of the transverse momentum distribution inside the jet cone [24, 69],

$$\rho(r) = \frac{1}{\Delta r}\frac{1}{N_{\rm jet}}\sum_{\rm jet}\frac{\sum_i p_T^i\left(r-\frac{1}{2}\Delta r, r+\frac{1}{2}\Delta r\right)}{\sum_i p_T^i(0,R)}, \tag{5}$$

measured from the parton distribution within the jet cone of the reconstructed jets, where $r=\sqrt{(\eta-\eta_{\rm jet})^2+(\phi-\phi_{\rm jet})^2}$ denotes the distance between the associate partons and the jet axis in the plane defined by pseudorapidity η and azimuthal angle ϕ. The total energy from the i-th jet within the circular annulus, defined by an inner radius $r_1=r-\Delta r/2$ and outer radius $r_2=r+\Delta r/2$, is given by $p_T^i(r_1,r_2)=\sum_{{\rm assoc}\in\Delta r}p_T^{\rm assoc}$, where $\Delta r=r_2-r_1$ represents the width of the annulus. Additionally, the total energy inside the jet cone with a radius R for the i-th jet is denoted by $p_T^i(0,R)$. The final result sums the total number of jets $N_{\rm jet}$ analyzed.

Our previous study on 2D jet tomography demonstrated that the jet shape broadening that was oberved correlates with the selection of jets exhibiting largerA_N^y values and lower $p_T^{\rm jet}$ in 0%−10% Pb+Pb collisions [49]. This observation indicates that jets originating from the central region of the QGP undergo the most significant medium-induced modifications, which can be explained by their extended propagation paths through the dense medium and the stronger jet quenching effects occurring at the higher temperatures characteristic of the QGP core region.

This study calculates the jet shapes corresponding to different centrality intervals. The upper panel of Fig. 4 presents the dependence of γ-jet shapes on the radius r in Pb+Pb collisions at $\sqrt{s_{NN}} = 5.02$ TeV across various centrality intervals (specifically 0%−10%, 10%−30%, 30%−50%, and 50%−90%), with comparisons made with jet shapes in p+p collisions. The lower panel shows the ratio of jet shapes between Pb+Pb and p+p collisions. Experimental observations reveal that, in both Pb+Pb and p+p collisions, all jet shapes exhibit a monotonic decrease with increasing radius r, indicating that the energy distribution within the jet cone is predominantly concentrated in the core region near the jet axis. By comparing jet shapes in p+p and Pb+Pb collisions, we observe that, across different centrality ranges, the jet shapes in Pb+Pb collisions are generally broader than those in p+p collisions. Moreover, within Pb+Pb collisions, the jet shapes in central collisions are broader than those in peripheral collisions. Numerical results in Fig. 4 demonstrate that, in Pb+Pb collisions, compared with p+p collisions, the transverse momentum lost by hard partons in the jet core region is partially transferred to soft medium-response particles at large angles relative to the jet axis. Furthermore, the differences in jet shapes among different centrality intervals suggest that jets originating from larger collision systems (*e.g.*, central collisions) undergo more significant medium modification effects owing to longer propagation paths, stronger jet quenching, and more prolonged evolution times.

Jets produced in different centrality intervals demonstrate distinct medium modification effects, as evidenced by the transverse momentum imbalance between $p_T^{\rm jet}$ and p_T^{γ}. The γ-jet transverse momentum imbalance is quantified by the ratio $X_{J\gamma} = p_T^{\rm jet}/p_T^{\gamma}$. Fig. 5 presents the γ-jet production rates as functions of $X_{J\gamma}$ for four centrality intervals (0%−10%, 10%−30%, 30%−50%, and 50%−90%) in Pb+Pb collisions at $\sqrt{s_{NN}} = 5.02$ TeV, with p+p collision results (dashed curve) provided for reference. Our calculations reveal that, compared with p+p collisions, the $X_{J\gamma}$ distributions for all four centrality intervals shift toward lower values, indicating jet quenching effects. Notably, jets from central collisions exhibit a more significant leftward shift in $X_{J\gamma}$ distributions than those from peripheral collisions, reflecting stronger quenching strength and medium modification effects in larger collision systems, which are consistent with previous discussions.

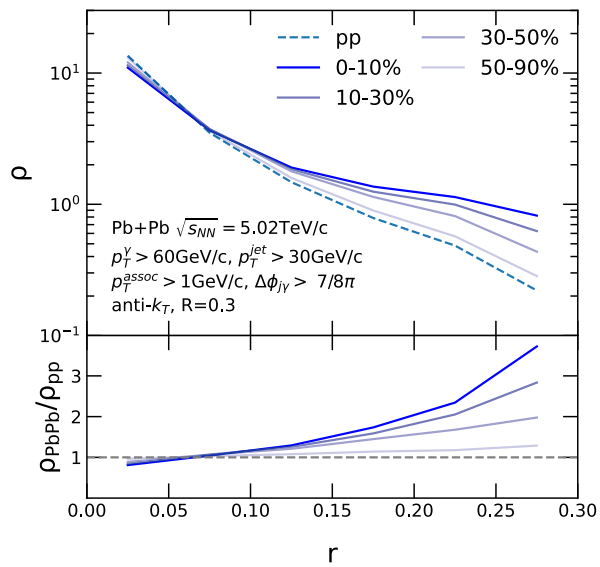

Fig. 4. (color online) Upper panel: jet shapes as functions of r, from different centrality intervals—0%−10%, 10%−30%, 30%−50%, and 50%−90%—in Pb+Pb and p+p collisions at $\sqrt{s_{NN}} = 5.02$ TeV. Lower panel: ratio of jet shapes in Pb+Pb collisions (for each centrality interval) to jet shapes in p+p collisions

B. Jet modification of γ-jet in Xe+Xe collisions

Furthermore, while comparing the QGP size differences between central and peripheral Pb+Pb collisions, we note that different nucleus-nucleus collision systems demonstrate significant variations in system size. In this study, we extended our investigation to include jet modifications in Xe+Xe collisions, a system characterized by smaller dimensions compared with Pb+Pb collisions.

Fig. 6 shows the γ-jet production rates as functions of A_N^y for different centrality intervals, specifically 0%−10%, 10%−30%, 30%−50%, and 50%−90%, in Xe+Xe collisions at $\sqrt{s_{NN}} = 5.44$ TeV. Similar trends are observed in Xe+Xe collisions, where the A_N^y distribution demonstrates a broader profile in central collisions compared with peripheral collisions. This observation indicates an enhanced transverse asymmetry of jets propagating parallel to the event plane, consistent with findings in

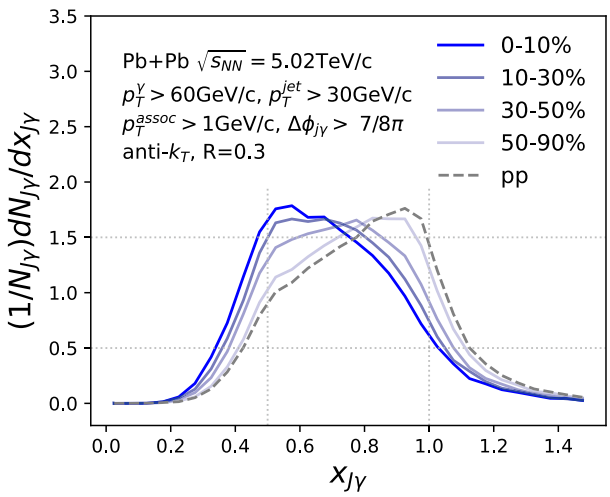

Fig. 5. (color online) $X_{J\gamma}$ distribution of γ-jets with four centrality intervals—0%−10%, 10%−30%, 30%−50%, and 50%−90%—in Pb+Pb and p+p collisions at $\sqrt{s_{NN}} = 5.02$ TeV

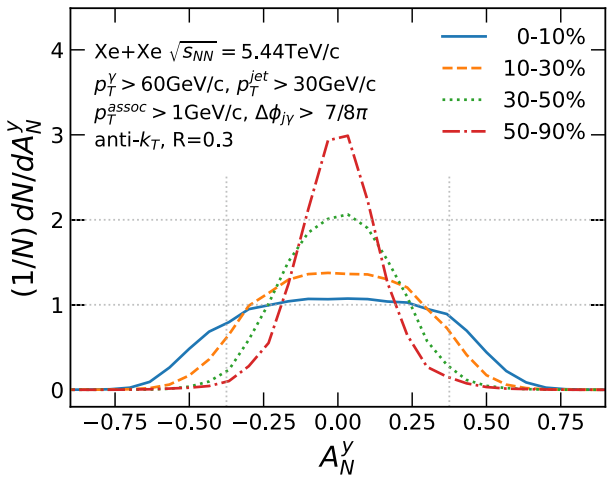

Fig. 6. (color online) γ-jet production rates $(1/N)\mathrm{d}N/\mathrm{d}A_N^y$ as functions of A_N^y, with four centrality intervals—0%−10%, 10%−30%, 30%−50%, and 50%−90%—in Xe+Xe and p+p collisions at $\sqrt{s_{NN}}$ = 5.44 TeV

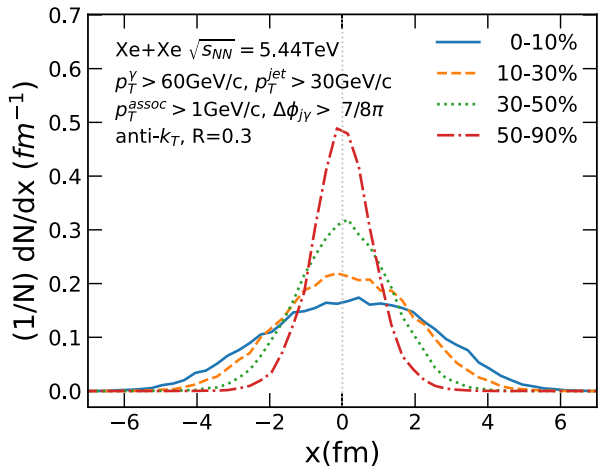

Fig. 7. (color online) γ-jet production rates $(1/N)\mathrm{d}N/\mathrm{d}A_N^y$ as functions of the initial jet production position x, with four centrality intervals, specifically 0%−10%, 10%−30%, 30%−50%, and 50%−90%, in Xe+Xe collisions at $\sqrt{s_{NN}}$ = 5.44 TeV

Pb+Pb collisions. Moreover, owing to the smaller system size in Xe+Xe collisions, the jet quenching strength and medium modification effects are weaker than in Pb+Pb collisions. Consequently, the A_N^y distribution is narrower in Xe+Xe collisions than in Pb+Pb collisions at the same centrality interval, particularly in central collisions. Similarly, the initial jet production position x exhibits a wider distribution in central Xe+Xe collisions than in peripheral Xe+Xe collisions, as shown in Fig. 7. Conversely, when comparing Xe+Xe and Pb+Pb collisions at the same centrality, the x distribution is broader in Pb+Pb collisions than in Xe+Xe collisions.

We also calculate the shapes of jets from different centrality intervals of Xe+Xe collisions. The upper panel of Fig. 8 shows the jet shapes as functions of the radius r, for γ-jets produced in different centrality intervals, specifically 0%−10%, 10%−30%, 30%−50%, and 50%−90% in Xe+Xe collisions at $\sqrt{s_{NN}}$ = 5.44 TeV, as compared with that in p+p collisions. The lower panel is the ratio of jet shapes between Xe+Xe and p+p collisions. Similar to Pb+Pb collisions, Xe+Xe collisions also exhibit centrality-dependent modifications in jet shapes, with more pronounced broadening observed in central collisions compared with peripheral ones. This observation indicates a gradual transition from strong to weak jet quenching effects and medium response as the collision centrality decreases. A systematic comparison between Pb+Pb and Xe+Xe systems further demonstrates that, at equivalent centrality intervals, jets in Pb+Pb collisions display broader shapes than their Xe+Xe counterparts. This distinction primarily originates from the larger system size in Pb+Pb collisions, which leads to stronger medium-induced modifications of jet properties relative to Xe+Xe collisions.

Finally, we examine the γ-jet transverse momentum

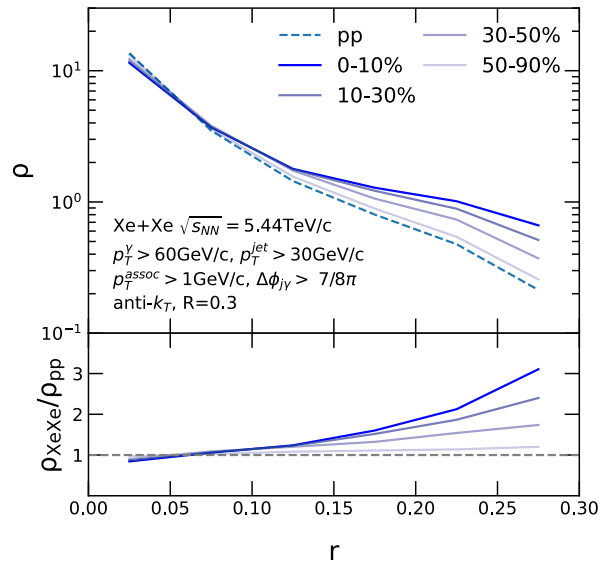

Fig. 8. (color online) Upper panel: jet shapes as functions of r, from different centrality intervals—0%−10%, 10%−30%, 30%−50%, and 50%−90%—in Xe+Xe and p+p collisions at $\sqrt{s_{NN}}$ = 5.44TeV. Lower panel: ratio of the jet shapes in Xe+Xe collisions (for each centrality interval) to the jet shape in p+p collisions

imbalance $X_{J\gamma}$ in Xe+Xe collisions across different centrality intervals, as shown in Fig. 9. Our calculations demonstrate that central collisions exhibit the most significant shift in the $X_{J\gamma}$ distribution toward lower values compared with p+p collisions, which reflects the strongest jet quenching effect. The magnitude of this shift diminishes in peripheral Xe+Xe collisions, consistent with reduced quenching strength in smaller collision systems. Notably, within equivalent centrality intervals, the $X_{J\gamma}$ distribution in Xe+Xe collisions shows less pro-

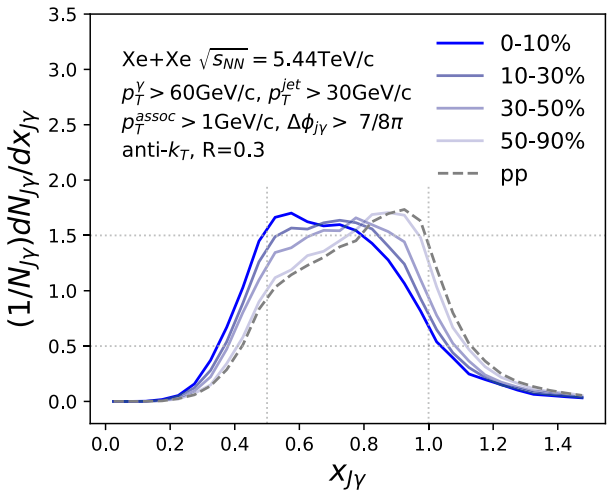

Fig. 9. (color online) $X_{J\gamma}$ distribution of γ-jets with four centrality intervals —0%−10%, 10%−30%, 30%−50%, and 50%−90%—in Xe+Xe and p+p collisions at $\sqrt{s_{NN}}$ = 5.44 TeV

nounced leftward shifting than that observed in Pb+Pb collisions. This systematic difference indicates comparatively weaker jet quenching in Xe+Xe systems, which is consistent with their smaller geometrical size relative to Pb+Pb collisions. We note that, in this section, apart from the results presented in Fig. 3 and Fig. 7, all other results can, in principle, serve as experimental observables.

IV. SUMMARY

In this study, we examined the medium modifications of γ-jets across various system sizes, particularly in different centrality intervals during Pb+Pb collisions at $\sqrt{s_{NN}}$ = 5.02 TeV and Xe+Xe collisions at $\sqrt{s_{NN}}$ = 5.44 TeV. The LBT model was utilized to simulate the propagation of jet partons within the QGP medium. Concurrently, the CLVisc hydrodynamic model, in conjunction with the TRENTo initial condition model, was employed to simulate the evolution of the QGP medium across varying centrality intervals in both Pb+Pb and Xe+Xe collisions. We conducted a comparative analysis of the medium modifications of γ-jets originating from collision systems of diverse sizes. These size variations are contingent upon distinct centrality intervals and the nature of the colliding nucleus, whether it is Pb or Xe. Our numerical findings indicate that, in nucleus-nucleus collisions, jets emanating from central collisions—associated with larger collision systems —demonstrate markedly enhanced medium modifications and increased jet quenching strength relative to those originating from peripheral collisions, typical of smaller collision systems. These findings not only lead to a broader distribution of the jet transverse asymmetry, denoted as A_N^y, and the initial jet production position, represented by x, but also result in a more expanded jet shape. Moreover, for jets originating from central collisions, there is a distinct shift toward smaller values of $X_{J\gamma}$ in the distribution of γ-jet transverse momentum imbalance, also represented by $X_{J\gamma}$. Within the same centrality interval, Pb+Pb collisions display a larger system size than Xe+Xe collisions, resulting in more pronounced jet quenching strength and medium modification effects. Consequently, jets in Pb+Pb collisions within this interval show wider distributions of both the jet transverse asymmetry, denoted as A_N^y, and the initial jet production position, represented by x. Additionally, they exhibit a broader jet shape and a more imbalanced distribution of $X_{J\gamma}$ compared with Xe+Xe collisions. We anticipate that future experiments investigating the medium modification and asymmetric features of jets will provide valuable insights into the properties of jet transport and the responses of the medium.

ACKNOWLEDGMENTS

The authors would like to thank Xin-Nian Wang for stimulating discussions. We thank Liqiang Zhu for providing the CLVisc data.

References

[1] M. Gyulassy and M. Plumer, Phys. Lett. B **243**, 432 (1990)
[2] X.-N. Wang and M. Gyulassy, Phys. Rev. Lett. **68**, 1480 (1992)
[3] G.-Y. Qin and X.-N. Wang, Int. J. Mod. Phys. E **24**, 1530014 (2015)
[4] A. Adare *et al.* (PHENIX), Phys. Rev. Lett. **105**, 142301 (2010)
[5] C. Adler *et al.* (STAR), Phys. Rev. Lett. **89**, 202301 (2002)
[6] B. Abelev *et al.* (ALICE), Phys. Lett. B **719**, 18 (2013)
[7] G. Aad *et al.* (ATLAS), Phys. Lett. B **707**, 330 (2012)
[8] S. Chatrchyan *et al.* (CMS), Phys. Rev. Lett. **109**, 022301 (2012)
[9] A. M. Sirunyan *et al.* (CMS), Phys. Lett. B **776**, 195 (2018)
[10] Y. Li, S. Shen, S. Wang *et al.*, Nucl. Sci. Tech. **35**, 113 (2024)
[11] E. Wang and X.-N. Wang, Phys. Rev. Lett. **89**, 162301 (2002)
[12] I. Vitev, J. Phys. G **30**, S791 (2004)
[13] H. Zhang, J. F. Owens, E. Wang *et al.*, Phys. Rev. Lett. **98**, 212301 (2007)
[14] H. Zhang, J. F. Owens, E. Wang *et al.*, Phys. Rev. Lett. **103**, 032302 (2009)
[15] I. Vitev and B.-W. Zhang, Phys. Rev. Lett. **104**, 132001 (2010)
[16] G.-Y. Qin and B. Muller, Phys. Rev. Lett. **106**, 162302 (2011)
[17] Y. He, I. Vitev, and B.-W. Zhang, Phys. Lett. B **713**, 224 (2012)
[18] C. Young, B. Schenke, S. Jeon *et al.*, Phys. Rev. C **84**, 024907 (2011)

[19] J. Barata, J. G. Milhano, and A. V. Sadofyev, Eur. Phys. J. C **84**, 174 (2024)
[20] J. Adams *et al.* (STAR), Phys. Rev. Lett. **97**, 162301 (2006)
[21] J. Casalderrey-Solana, J. G. Milhano, and U. A. Wiedemann, J. Phys. G **38**, 035006 (2011)
[22] K. Aamodt *et al.* (ALICE), Phys. Rev. Lett. **105**, 252301 (2010)
[23] G. Aad *et al.* (ATLAS), Phys. Rev. Lett. **105**, 252303 (2010)
[24] A. M. Sirunyan *et al.* (CMS), Phys. Rev. Lett. **122**, 152001 (2019)
[25] R. Baier, Y. L. Dokshitzer, A. H. Mueller *et al.*, Nucl. Phys. B **484**, 265 (1997)
[26] R. Baier, Y. L. Dokshitzer, A. H. Mueller *et al.*, Nucl. Phys. B **483**, 291 (1997)
[27] R. Baier, Y. L. Dokshitzer, A. H. Mueller *et al.*, Nucl. Phys. B **531**, 403 (1998)
[28] X.-f. Guo and X.-N. Wang, Phys. Rev. Lett. **85**, 3591 (2000)
[29] X.-N. Wang and X.-F. Guo, Nucl. Phys. A **696**, 788 (2001)
[30] J. Casalderrey-Solana and X.-N. Wang, Phys. Rev. C **77**, 024902 (2008)
[31] A. Majumder, Phys. Rev. D **85**, 014023 (2012)
[32] D. Everett *et al.* (JETSCAPE), Phys. Rev. C **103**, 054904 (2021)
[33] D. Everett *et al.* (JETSCAPE), Phys. Rev. Lett. **126**, 242301 (2021)
[34] S. Cao *et al.* (JETSCAPE), Phys. Rev. C **104**, 024905 (2021)
[35] Q.-F. Han, M. Xie, and H.-Z. Zhang, Eur. Phys. J. Plus **137**, 1056 (2022)
[36] M. Xie, Q.-F. Han, E.-K. Wang *et al.*, Nucl. Sci. Tech. **35**, 125 (2024)
[37] M. Xie, W. Ke, H. Zhang *et al.*, Phys. Rev. C **108**, L011901 (2023)
[38] Y. He, L.-G. Pang, and X.-N. Wang, Phys. Rev. Lett. **122**, 252302 (2019)
[39] M. L. Miller, K. Reygers, S. J. Sanders *et al.*, Ann. Rev. Nucl. Part. Sci. **57**, 205 (2007)
[40] L. Pang, Q. Wang, and X.-N. Wang, Phys. Rev. C **86**, 024911 (2012)
[41] L.-G. Pang, H. Petersen, and X.-N. Wang, Phys. Rev. C **97**, 064918 (2018)
[42] B. Schenke, S. Jeon, and C. Gale, Phys. Rev. C **82**, 014903 (2010)
[43] B. Schenke, S. Jeon, and C. Gale, Phys. Rev. Lett. **106**, 042301 (2011)
[44] C. Gale, S. Jeon, B. Schenke *et al.*, Phys. Rev. Lett. **110**, 012302 (2013)
[45] S. Ryu, J. F. Paquet, C. Shen *et al.*, Phys. Rev. Lett. **115**, 132301 (2015)
[46] J. S. Moreland, J. E. Bernhard, and S. A. Bass, Phys. Rev. C **92**, 011901 (2015)
[47] W. Ke, J. S. Moreland, J. E. Bernhard *et al.*, Phys. Rev. C **96**, 044912 (2017)
[48] Y. He, L.-G. Pang, and X.-N. Wang, Phys. Rev. Lett. **125**, 122301 (2020)
[49] Y.-X. Xiao, Y. He, L.-G. Pang *et al.*, Phys. Rev. C **109**, 054906 (2024)
[50] D. Anderson (STAR), Acta Phys. Polon. Supp. **16**, 1 (2023)
[51] M. Xie, X.-N. Wang, and H.-Z. Zhang, Phys. Rev. C **103**, 034911 (2021)
[52] A. Luo, Y.-X. Mao, G.-Y. Qin *et al.*, Phys. Lett. B **837**, 137638 (2023)
[53] L. Chen, S.-Y. Wei, and H.-Z. Zhang, Eur. Phys. J. C **80**, 1136 (2020)
[54] Z. Yang, W. Chen, Y. He *et al.*, Phys. Rev. Lett. **127**, 082301 (2021)
[55] K. Aamodt *et al.* (ALICE), Phys. Rev. Lett. **105**, 252302 (2010)
[56] M. Sas, Rev. Mex. Fis. Suppl. **3**, 040915 (2022)
[57] G. Nijs, W. van der Schee, U. Gürsoy *et al.*, Phys. Rev. C **103**, 054909 (2021)
[58] S. Acharya *et al.* (ALICE), Phys. Lett. B **784**, 82 (2018)
[59] S. Acharya *et al.* (ALICE), Phys. Rev. Lett. **123**, 142301 (2019)
[60] B. G. Zakharov, Eur. Phys. J. C **78**, 427 (2018)
[61] H. Li, F. Liu, G.-l. Ma *et al.*, Phys. Rev. Lett. **106**, 012301 (2011)
[62] Y. He, T. Luo, X.-N. Wang *et al.*, Phys. Rev. C **91**, 054908 (2015)
[63] S. Cao, T. Luo, G.-Y. Qin *et al.*, Phys. Rev. C **94**, 014909 (2016)
[64] X.-N. Wang and Y. Zhu, Phys. Rev. Lett. **111**, 062301 (2013)
[65] S. Cao and X.-N. Wang, Rept. Prog. Phys. **84**, 024301 (2021)
[66] T. Luo, Y. He, S. Cao *et al.*, Phys. Rev. C **109**, 034919 (2024)
[67] Y. He, S. Cao, W. Chen, T. Luo *et al.*, Phys. Rev. C **99**, 054911 (2019)
[68] W. Chen, S. Cao, T. Luo *et al.*, Phys. Lett. B **777**, 86 (2018)
[69] T. Luo, S. Cao, Y. He *et al.*, Phys. Lett. B **782**, 707 (2018)
[70] B.-W. Zhang, E. Wang, and X.-N. Wang, Phys. Rev. Lett. **93**, 072301 (2004)
[71] T. Sjostrand, S. Mrenna, and P. Z. Skands, JHEP **2006**(05), 026 (2006)
[72] T. Sjostrand, S. Mrenna, and P. Z. Skands, Comput. Phys. Commun. **178**, 852 (2008)
[73] M. Cacciari, G. P. Salam, and G. Soyez, Eur. Phys. J. C **72**, 1896 (2012)
[74] M. Cacciari and G. P. Salam, Phys. Lett. B **641**, 57 (2006)